

Coulomb blockade conductance peak fluctuations in quantum dots and the independent particle model

Raul O. Vallejos¹, Caio H. Lewenkopf[†], and Eduardo R. Mucciolo²

¹ Instituto de Física, Universidade do Estado do Rio de Janeiro,
R. São Francisco Xavier 524, 20559-900 Rio de Janeiro, Brazil

² Departamento de Física, Pontifícia Universidade Católica do Rio de Janeiro,
Caixa Postal 38071, 22452-970 Rio de Janeiro, Brazil

(April 15, 2024)

Abstract

We study the combined effect of finite temperature, underlying classical dynamics, and deformations on the statistical properties of Coulomb blockade conductance peaks in quantum dots. These effects are considered in the context of the single-particle plus constant-interaction theory of the Coulomb blockade. We present numerical studies of two chaotic models, representative of different mean-field potentials: a parametric random Hamiltonian and the smooth stadium. In addition, we study conductance fluctuations for different integrable confining potentials. For temperatures smaller than the mean level spacing, our results indicate that the peak height distribution is nearly always in good agreement with the available experimental data, irrespective of the confining potential (integrable or chaotic). We find that the peak bunching effect seen in the experiments is reproduced in the theoretical models under certain special conditions. Although the independent particle model fails, in general, to explain quantitatively the short-range part of the peak height correlations observed experimentally, we argue that it allows for an understanding of the long-range part.

I. INTRODUCTION

Since the first electronic transport measurements in semiconductor quantum dots in the Coulomb blockade regime were made,¹ a significant amount of data has been accumulated. The appropriate theoretical model used in understanding this data depends on the size of the electronic island. Two situations arise. When dealing with small or very small systems, where the number of electrons N in the Coulomb island is of the order of 10 (or a maximum of 10^2), the self-consistent approach is successful.² In this regime the environment generates a smooth, nearly parabolic potential and most of the quantum dot properties can be understood in terms of an unsophisticated self-consistent electronic structure calculation. On the other hand, the most adequate theoretical description for data taken from larger systems, with N of order 10^3 (or at least larger than 10^2), is statistical. In distinction to the first case, for large dots the confining potential is no longer expected to be parabolic up to energies close to the Fermi surface. In fact, in large gated structures, the dot geometrical shape can be substantially modified by adjusting voltages. Within the single-particle picture, it is believed that the complexity of the confining potential yields a chaotic motion in the classical limit, thus justifying a quantum mechanical modeling based on a statistical theory.^{3,4} Further arguments for such approach are provided by the influence of weak disorder and the fact (not always justifiable) that many-body correlations should bring only small corrections to the usual single-particle description of transport.

The single-particle statistical theory^{5,7} is widely accepted because of its early success in predicting the distribution of peak heights in the single-channel tunneling regime, later experimentally confirmed.^{8,9} In the regime where the mean level spacing is much larger than $k_B T$, the predicted distribution of peak heights is strongly non-Gaussian and clearly peaked towards zero values. While the single-particle plus constant interaction theory captures most qualitative aspects observed in the experiments, some quantitative aspects defy comprehension. Perhaps the most celebrated one is the absence of Wigner-Dyson fluctuations in the conductance peak spacings.^{10,12}

There is also an important and rather prominent feature of the experimental data which is less discussed in the literature and remains unexplained: the notable clustering of peaks with similar heights. That is, in most experiments (an important exception is Ref. 8), by sweeping the gate voltage, large and small peaks tend to appear in bunches, indicating the existence of peak to peak correlation. This is at odds with the statistical single-particle theory at low temperatures, which associates to each peak an independent single-particle eigenstate. A recent experiment¹³ showed yet another puzzling feature: the correlation tends to increase with temperature and the slope depends on the dot area (for a small dot it saturated at $k_B T = 2$.)

Any successful theoretical model describing all these issues has to take into account that each conductance peak corresponds to a system containing a different number of particles. As electrons are added to the quantum dot the gate voltage configuration varies and the confining potential changes accordingly.¹⁴ Furthermore, and probably even more important, the additional particles change the electron mean field. Although not the original idea addressed in Ref. 14, we can parameterize the total change in the single-particle energies and wave functions by moving from one peak to the next through a parametric variation

X which takes into account changes of the external and mean field potentials. We can call

it the mean-field "deformation". Although difficult to quantify, X is obviously nonzero.

In this paper we concentrate on the statistical measures of the conductance peak heights, namely their distribution and autocorrelation function. We use the constant interaction plus independent particle model to discuss the role of "deformations" and temperature. We show that for $k_B T$ the theoretical peak height distribution agrees with the experimental data for systems with chaotic underlying dynamics, irrespective of the deformation parameter. We also show a very reasonable agreement between chaotic and some integrable models for $k_B T > 0.25$. As for the peak height autocorrelation function, we could not find any robust and generic mechanism to explain the strong peak to peak correlations seen in some experiments. We were only able to find such correlations for special choices of lead positions.

The structure of this paper is as follows. In section II we begin with a short review of the constant interaction model, which is used throughout this work, centered on a discussion about finite temperature corrections and parametric variations. In section III we study the combined effect of temperature and deformations in a random matrix model. In section IV we investigate dynamical mechanisms to explain the observed correlations between peak heights. The proposed mechanisms are examined by studying a suitable dynamical model. The influence of data set sizes on the evaluation of peak height correlations is critically discussed in section V. Having analyzed only chaotic dynamical systems, we investigate in section VI whether the experiments carried out so far indeed observed fingerprints of chaos. Insight on this question is obtained by studying the peak height distribution for a few integrable models. Finally, we summarize our conclusions in section VII.

II. THE SINGLE-PARTICLE PLUS CONSTANT INTERACTION MODEL FOR QUANTUM DOTS

The theoretical description used in this study is based on the so-called independent particle plus "constant interaction" (CI) model,¹ where the electron-electron interaction is taken into account through a fixed (capacitive) charging energy term in the Hamiltonian:

$$H = \sum_{i=1}^N \frac{p_i^2}{2m} + V(r_i) + \frac{U}{2} N(N-1) + e V_g N; \quad (1)$$

where N is the total number of electrons with effective mass m in the dot, U is the charging energy, and V_g is some tunable gate voltage. The coefficient is a function of the capacitance matrix elements of the dot.¹⁵ The single particle potential in Eq. (1) accounts only for the electrostatic confinement and background disorder.

When the dot is in equilibrium with the reservoirs represented by the leads, its total energy is minimal for a certain value of N . The precise value of N depends on the dot conning geometry, chemical potential (Fermi energy) in the reservoirs, and gate voltage V_g . The electronic many-body ground state wave function is given by the Slater determinant of all bounded single-particle eigenstates with energies smaller than the Fermi energy. In its crudest version, the single-particle states in the CI model are determined by the bare electron conning potential alone. It has been argued^{16,20} that many-body effects are important and one should instead get the single-particle states from a mean-field approximation, such

as Hartree-Fock. We will not attempt to answer this question in this work, but rather comprehensively study most features that may be traced to one-body effects.

Both single-particle eigenenergies and eigenfunctions influence the electronic transport through the quantum dot. The wave functions, in particular, enter into the standard formulation⁵ through the partial decay widths $\Gamma_p^{r,l}$ which quantify the connectivity between the eigenstate in the dot and the electronic states in the leads (r and l stand for right and left leads, respectively). In the regime of thermally broadened resonances and large charging energy, $\Gamma_p^{r,l} \ll k_B T \ll U$, linear response theory yields the following expression for the two-point conductance of a dot (weakly) coupled to reservoirs⁵

$$G = \frac{e^2}{h k_B T} \sum_{p=1}^N \frac{\Gamma_p^l \Gamma_p^r}{\Gamma_p^l + \Gamma_p^r} F_{\text{eq}}(\mu_p, N) \left[1 - f\left(\frac{E_p - \mu_N}{k_B T}\right) \right] f\left(\frac{E_p - \mu_N}{k_B T}\right) \quad (2)$$

with $E_p = \epsilon_p + U(N-1) - e\phi = \mu_F$. The sum runs over all single-particle states p with energies ϵ_p and partial decay widths Γ_p^r and Γ_p^l . The latter describe the electron tunneling out of the dot and into the reservoirs, or vice-versa. Thus, the total tunneling rate is $\Gamma_p = \Gamma_p^l + \Gamma_p^r$. $F_{\text{eq}}(\mu_p, N)$ is the canonical occupation probability of the level p for a dot containing N electrons in thermal equilibrium. f is the Fermi-Dirac distribution, $f(\mu) = 1/[1 + \exp(\mu/k_B T)]$, S is the entropy of the dot, and μ_F is the Fermi energy in the reservoirs. We will specialize our discussion to spin split (nondegenerate) energy levels.

In experiments, sequences of conductance peaks are observed by varying the external gate voltage V_g , thus changing the electrostatic energy in the dot. Within the CIM model, in the single-level tunneling regime, where $\Gamma_p^{r,l} \ll k_B T$, and as the gate potential is swept, conductance peaks occur whenever the resonance condition

$$E(N+1) - E(N) = \mu_F \quad (3)$$

is satisfied.⁵ Here $E(N)$ is the ground state energy of the dot containing N electrons. Within the constant interaction model, Eq. (3) can be rewritten as

$$\epsilon_N + (N-1)U - e\phi = \mu_F; \quad (4)$$

ie., $E = 0$. We remark that, although correct at the level of the Hartree-Fock approximation (with $N-1$), it is still a matter of debate in the literature whether Eq. (4) is generally valid.^{16,22} The existence of many-body correlation effects may lead to a breakdown of Kohn-Sham's theorem and a different resonance condition. Furthermore, the strong assumption of a constant U prevents an adequate description of fluctuations in peak position. Nevertheless, these restrictions shall not affect our discussion on the statistics of peak heights in the single-particle approximation.

In order to make the notation more compact, let us rescale the conductance to a dimensionless form,

$$G = \frac{e^2}{h} \frac{h}{4k_B T} g; \quad (5)$$

Moreover, for the sake of simplicity, we consider that the average decay widths (taken over many resonances) are equal: $\hbar \Gamma_i = \hbar \Gamma_l = \hbar \Gamma$. In the temperature regime where $\hbar \Gamma \ll k_B T$, the resonance condition, combined with Eq. (2), results in the well-known expression for the single-level conductance peak height,

$$G_P^{\text{max}} = \frac{1}{\hbar \Gamma} \frac{\frac{1}{\Gamma_P} \frac{\Gamma}{\Gamma_P}}{\frac{1}{\Gamma_P} + \frac{\Gamma}{\Gamma_P}} : \quad (6)$$

Assuming that the electronic dynamics inside the dot is classically chaotic, Jalabert and collaborators⁶ used a random matrix model to calculate the distribution of partial decay widths in this temperature regime, in the presence ($\gamma = 2$) or not ($\gamma = 1$) of an applied magnetic field. They obtained

$$P(\Gamma^{(l)}) = \frac{C}{2 \Gamma^{(l)}} \frac{\Gamma^{(l) \gamma - 2}}{2 \hbar \Gamma^{(l) \gamma}} \exp \left(-\frac{\Gamma^{(l) \gamma}}{2 \hbar \Gamma^{(l) \gamma}} \right) ; \quad (7)$$

where C is a normalization constant that can be expressed in terms of the gamma function: $C = \Gamma(\gamma) \Gamma(\gamma/2)$. By further assuming that the contacts are sufficiently far from each other so that Γ and Γ_l are uncorrelated, expressions were derived for the distribution of dimensionless peak heights, namely,

$$P_{\gamma=1}(\gamma) = \frac{\gamma}{2} e^{-\gamma/2} \quad (8)$$

and

$$P_{\gamma=2}(\gamma) = 4 \frac{\gamma}{K_0(2\gamma)} + K_1(2\gamma) e^{-\gamma} ; \quad (9)$$

where $K_0(x)$ and $K_1(x)$ are modified Bessel functions. These predictions were later experimentally confirmed by two independent experiments.^{8,9} Equations (8) and (9) will serve us as benchmarks in later sections.

As mentioned in the introduction, the early success of the random matrix hypothesis^{6,7} in explaining statistical properties of conductance peaks in quantum dots seemed somewhat inconsistent. The experimental confirmation of theoretical prediction of the distribution $P(\gamma)$ contrasts with the observation of strong correlations between successive peak heights in most data sets.^{9,13} Recall that standard random matrix theory (RMT)²³ leads to uncorrelated eigenfunctions, giving conductance peaks with a similar property. However, the fact that the condition $\hbar \Gamma \ll k_B T$ is hardly achieved in the early experiments suggests that the discrepancy could be related to a finite temperature effect. The inclusion of finite temperature in RMT was carried out by Alhassid and collaborators²⁴ by computing the canonical occupation factors $F_{\text{eq}}(\Gamma_P, \Gamma)$ in Eq. (2). Already for $k_B T \approx 0.3$ they observed significant temperature corrections in $P(\gamma)$, as compared to Eq. (9). The corrections, however, fail to quantitatively reproduce the available experimental data,¹³ and the discrepancy grows larger as temperatures goes beyond $\hbar \Gamma$. We will return to this point later.

The canonical average necessary to calculate $F_{\text{eq}}(\Gamma_P, \Gamma)$ can be taken either by explicit summation of all possible single-particle configurations, as recently done in Ref. 25, or in a

quadrature approximation for the canonical partition function, as in Refs. 24,26. We adopt the latter approach in what follows. The procedure consists in expressing the canonical partition function as

$$Z_N = \frac{e^{E^{\text{tot}}(N)=k_B T} X^L Y^{\frac{L}{2}}}{L} \prod_{j=1}^{N+\frac{L}{2}} \left(1 + e^{i j - 1 - \frac{j}{k_B T} \epsilon_j} \right); \quad (10)$$

where $j = 2 \dots N+\frac{L}{2}$, $E^{\text{tot}}(N) = \sum_{p=N-\frac{L}{2}}^{N+\frac{L}{2}} \epsilon_p$, and

$$X = \begin{cases} 1; & (1 \leq N) \\ 1; & (1 > N); \end{cases} \quad (11)$$

with L standing for the number of states taken into account (we are interested in the case where $N \leq L-1$). This form of organizing the sum, involving only exponentially decaying terms, together with the choice $\epsilon = (\epsilon_N + \epsilon_{N+1})/2$, guarantees fast convergence. The free energy and the entropy are straightforwardly evaluated from Eq. (10) recalling that $F(N) = -k_B T \ln Z_N = E^{\text{tot}}(N) - TS(N)$. With the quadrature approximation, the calculation of the canonical occupation number is carried according to

$$F_{\text{eq}}(\epsilon_p, N) = \frac{e^{S(N)=k_B T} X^L Y^{\frac{L}{2}}}{L} \prod_{j=1}^{N+\frac{L}{2}} \left(1 + e^{i j - 1 - \frac{j}{k_B T} \epsilon_j} \right) \frac{1}{1 + e^{i j - 1 - p + \frac{j}{k_B T} \epsilon_j}}; \quad (12)$$

Since we are only interested in the statistics of conductance peak maxima and not of spacings, we introduce in Eq. (2) the resonance condition for $k_B T \ll \epsilon$ [Eq. (4)]. In the limit of strong Coulomb blockade $k_B T \ll e^2/C$, this yields⁵

$$G_N = \frac{4}{h} \sum_{p=N-\frac{L}{2}}^{N+\frac{L}{2}} \frac{1}{\frac{1}{p} + \frac{r}{p}} F_{\text{eq}}(\epsilon_p, N) [1 - f(\epsilon_p - \epsilon_N)] f((\epsilon_p - TS(N)) + TS(N - 1)); \quad (13)$$

One further remark about the implementation of Eq. (10) is in order. In our numerical simulations we varied the number of eigenstates L summed over depending on the temperature range. For $k_B T \leq 0.1$, we found that as few as 4 were sufficient to achieve good convergence; for higher temperatures, $k_B T \geq 0.1$, we used as many as 20.

In the experimental setups where plunger gates are used to define both shape and depth of the confining potential, one expects that variations in the potential V_g will continuously deform the dot.²⁷ This situation is met in lateral quantum dots, where most of the data were taken^{8,9,11,13} (an important exception is Ref. 28). Furthermore, as pointed out in the introduction, as one adds electrons to the dot the mean field also changes. Thus, to establish theoretically the direct relation between V_g and the dot electronic mean field

it is necessary to know the experimental set up in detail and perform rather sophisticated numerical simulations. While such study is desirable, it is not crucial for our analysis and will not be pursued here. We therefore simplify the problem parameterizing the "deformations" by a generic variable X on which eigenvalues and eigenfunctions will depend. In summary, the key point behind this hypothesis is that by adding one extra electron to the dot the mean electrostatic potential changes parametrically, on average, by X .¹⁴ In this way, the N th conductance peak involves a sum over eigenvalues and partial widths $f_p''(X); \frac{r}{p}(X); \frac{1}{p}(X)g$, while the next peak in the sequence will depend on $f_p''(X + X); \frac{r}{p}(X + X); \frac{1}{p}(X + X)g$. It is convenient to measure the deformations in units of the typical distance between energy level anti-crossings, namely, the inverse root mean square derivative of the energy levels with respect to deformations:²⁹

$$X_c = \frac{2}{4} \frac{d_p''}{dX} \frac{1}{2} + \frac{2}{5} \frac{d_p''}{dX} \frac{3}{1=2} : \quad (14)$$

(Here $\langle \dots \rangle$ stands for an average over states p and over the parameter X). When the addition of a single extra electron is enough to scramble strongly energy levels and wave functions, $X_c \approx X_{c-1}$. In this circumstances, we expect each new conductance peak to signal a different and independent realization of the effective confining potential in the dot. Thus, in the regime of strong deformations, peaks heights should be fairly uncorrelated, in contrast with what happens as temperature is increased. A systematic study of temperature and shape deformation combined is carried out below.

III. THE EFFECT OF PARAMETRIC VARIATIONS ON THERMAL AVERAGES

In this section we investigate the effect of parametric Hamiltonian variations on thermal averages. More specially, we are interested in answering two questions: (a) Are the correlations between consecutive peak heights sensitive to shape deformations? (b) What is the effect of parametric variations on the distribution of peak heights? We assume that the electronic underlying classical dynamics is fully chaotic and, therefore, its quantum Hamiltonian can be modeled by a random matrix. In doing so, we restrict our analysis to universal aspects; we leave the study of some specific dynamical models and nonuniversal features to the following sections. Since a fully analytical treatment of the problem is not available, we implement the numerical procedure discussed in the Sec. II to evaluate the canonical averages from a given sequence of energy levels and tunneling rates.

The set of eigenenergies and eigenfunctions of a random parametric Hamiltonian can be conveniently obtained from a Hermitian matrix of the form

$$H(X) = H_1 \cos X + H_2 \sin X; \quad (15)$$

where H_1 and H_2 are independent $N \times N$ matrices ($N = 500$ in our calculations) belonging to the proper Gaussian ensemble. In our numerical calculations, the orthogonal ensemble (GOE, $\beta = 1$) was used to model the situation when no magnetic field is present (time-reversal symmetric systems). For the case with non-zero magnetic field and broken time-reversal symmetry, we used instead the unitary ensemble (GUE, $\beta = 2$). For each realization

of H_1 and H_2 and a given value of the parameter X , the matrix $H(X)$ was diagonalized through standard methods. Only the 100 central eigenvalues were kept after each diagonalization. This was done in order to avoid large density variations in the spectra and the consequent need for unfolding, as well as the inclusion of localized eigenstates from the tails of the band. The resulting eigenfunctions $f_p(k; X)$ were used to generate the right and left tunneling rates according to the point contact approximation $\Gamma_p^r(X) / j_p(k=1; X)^2$ and $\Gamma_p^l(X) / j_p(k=N; X)^2$. The energy eigenvalues $f_p(X)$ were used in the quadrature approximation for the canonical partition function given by Eq. (10). Thus, for a given realization of H_1 and H_2 , a certain deformation X , and temperature T , we simulated sequences of dimensionless conductance peak heights as given by Eq. (13).

It is noteworthy that the calculation shown in Ref. 24, although similar in formulation to ours, relied only on the randomness of the tunneling rates and neglected fluctuations in the eigenenergies by adopting a picket-fence approximation for the spectrum. Here, instead, we use eigenenergies fully consistent with the Wigner-Dyson statistics predicted from RMT. For the unitary case, due to the strong level repulsion the picket-fence is a reasonable first approximation for the spectrum and we expect our results to be similar to those of Ref. 24. Indeed we observe only small, 10% differences in peak height correlation functions (see below). For the orthogonal case, however, level repulsion is weaker and to obtain accurate results it is recommended to use the exact spectrum. This issue becomes very important when calculating $F_{eq}(N)$ for dynamical systems. In Sec. IV we shall resume this discussion.

The results presented here involved data obtained from 50 independent realizations of the matrices H_1 and H_2 . For each of these realizations, 150 values of X were used within the interval $[0; \pi/2]$ to generate peak sequences related to different "shape" deformations. Additional statistics was obtained by varying the "chemical potential" (i.e., the initial number of electrons in the dot) and the "original shape" (i.e., the initial X point), taking care to avoid introducing spurious correlations between distinct peak sequences.

As an illustration, three typical sequences of conductance peak maxima are shown in Fig. 1 for the orthogonal ensemble with some arbitrary deformation. Notice that, as temperature increases, the overall modulation becomes more pronounced, marking the existence of large peak-to-peak correlations. The clustering of peaks with similar heights is characteristic of the dominance of a single well-connected eigenstate over a wide energy range.

The most characteristic feature of the thermal average is that the occurrence of small peaks becomes unlikely, even for temperatures which are smaller than β . This can be observed in the curves presented in Ref. 24 for the distribution of peak heights, although the effect is not always quantitatively confirmed by the experiments. For instance, in the case of preserved time-reversal symmetry the absence of small peaks should be very pronounced, in clear contradiction with the currently available experimental data.^{8,9}

To start a quantitative analysis, let us first concentrate on the correlation of peak heights between neighboring conductance peaks. For this purpose, we have calculated the correlation function

$$c(n) = \frac{h_{N+n} - \bar{h}_N}{h_N - \bar{h}_N}; \quad (16)$$

where $\bar{h}_N = \frac{1}{N} \sum_{i=1}^N h_N i$ represents the deviation from average height of the N th peak. The

averages $\langle \dots \rangle_i$ are taken over different realizations of H_2 , as well as over N . The results for each Gaussian ensemble at different temperatures and deformations are shown in Figs. 2 and 3. Notice that even small parametric changes in the Hamiltonian can rapidly destroy the correlation of peak heights obtained from thermal averaging. This effect can be made more quantitative by calculating the halfwidth at halfmaximum (HWHM) of the correlator $c(n)$ as a function of temperature (see Fig. 4).

Small deformations \propto exclusively due to shape variations are reported in a recent experiment¹³ where, in addition, a theoretical curve solely based on "static" Gaussian ensembles ($\propto = 0$) is used to explain the data. Although the parametric deformation for this experimental set up is relatively small, one should not disregard its importance: For $\propto = 0.3$ we already observe in Fig. 4 a much slower increase in correlation versus temperature than for $\propto = 0$, in agreement with the data of Ref. 13. A fully consistent, parametric RMT for the peak height fluctuations yields a smaller correlation length than what is predicted by the "static" Gaussian ensembles. This is a clear indication that the theoretical curve shown together with the correlation length data in Ref. 13 should be taken with reservation. Nevertheless, the inclusion of parametric deformations alone does not solve the discrepancy between the RMT predictions and the experimental data at small temperatures.

Another important statistical measure of the peak height fluctuation is its distribution. In Figs. 5 and 6 we show the distributions for both GOE and GUE cases. The inset illustrates the dependence on deformations for a given temperature. We observe that, contrary to the correlation lengths of peak heights, the distributions are not affected by parametric deformations, but do depend strongly on temperature. For $k_B T \rightarrow 0$ the distribution moves towards a Gaussian shape. It is important to notice that RMT captures the qualitative aspects of the temperature dependence observed experimentally,¹³ but fails quantitatively: The data shows a smaller fluctuation in peak heights at high temperatures ($k_B T > \dots$) than the theory predicts. This could be interpreted as an indication that for such temperatures many-body (or dephasing) effects become important.¹³

We conclude that a theory based solely on random matrices with a proper thermal average is not capable of explaining simultaneously the peak height distribution and correlations. Even before attempting to improve the theory by including many-body interaction effects, we shall investigate whether nonuniversal aspects of the underlying single-particle dynamics also play an important role and lead to additional peak height correlation mechanisms.

IV. DYNAMICAL CORRELATIONS IN CHAOTIC SYSTEMS

In this section we investigate how single-particle dynamical correlations statistically influence the conductance peak heights. We first examine how universal chaotic wave function correlations^{30,33} manifest on the conductance autocorrelation function. These correlations go beyond RMT theory, but are universal in the sense that they arise for any chaotic quantum state with finite wavelength. We show analytically that at $T = 0$ the effect is small, but is enhanced at higher temperatures. We also investigate if peak height bunching can be explained by eigenstates localized in coordinate space. Such localization corresponds to wave functions with amplitudes concentrated along certain periodic orbits of the underlying classical Hamiltonian. This non-universal, spatial structure is known in the quantum chaos

literature as a \scar"³⁴ of the classical dynamics on the wave functions.

We illustrate our investigation by studying numerically a suitable dynamical model. Namely, we calculate $P(\epsilon)$ and $c(n)$ for the smooth stadium potential as a function of T and deformation. We also model the coupling between the dot and the leads in two distinct ways. Most of the results presented below assume point contacts, in which case $\Gamma_p = |j_p(r_c)|^2$, where $j_p(r_c)$ is the p -th dot eigenfunction, evaluated at some point r_c in the interface region between dot and lead. This description implies that, close to the dot, the leads should be narrow and carry a single propagating channel. Alternatively, we use the standard R-matrix formalism to calculate the decay width for extended leads by taking the overlap integral over the contact area: $\Gamma_p = \int_{\text{contact}} |c(r)|^2 |j_p(r_c)|^2$, where c is the channel wave function. Both models assume that the barrier penetration factors are small, such that $\hbar \ll \dots$. Furthermore, it is assumed that the penetration factors vary smoothly with energy and can thus be incorporated in \hbar without affecting fluctuations.

A. Corrections to the conductance fluctuations due to wave function correlations

A recent work by Narimanov and collaborators³⁵ explored the idea that the short time dynamics can influence peak height conductance fluctuations. Using the semiclassical theory they derived a correction to the conductance in the absence of magnetic field and $k_B T = 0$ which provides a particularly strong effect on the tails of the autocorrelation function. One of the important constraints in Ref. 35 is that the results are obtained for symmetrically placed leads, such that $r = -1$. Our study addresses a more generic situation and has a different starting point than theirs.

In 1977, Berry³⁰ suggested that wave functions of billiards with a chaotic underlying dynamics can be statistically described by a random superposition of plane waves with a fixed energy. As a result, he found that chaotic wave functions at energy E display universal spatial correlations. In two dimensions the result is

$$C(r_1; r_2; E) = A^{-1} J_0(k|r_1 - r_2|); \quad (17)$$

where A is the billiard area, $\hbar k = (2m E)^{1/2}$, and $J_0(x)$ is the ordinary Bessel function. Numerical verifications of Eq. (17) usually use an arbitrary wave function, fix one coordinate and average over all directions to obtain $C(r; E)$, with $r = |r_1 - r_2|$. Alternatively, and closely related to this study, $C(r; E)$ can be obtained by keeping r_1 and r_2 fixed and taking the average over wave functions corresponding to eigenenergies close to E (see for instance, Ref. 36 and references therein).

Since wave functions are spatially correlated, so are ϵ^1 and ϵ^r . The joint probability distribution of ϵ^r and ϵ^1 has already been obtained in the orthogonal case ($\beta = 1$) by the supersymmetric technique.³¹ Srednicki³³ later derived the same quantity by elegantly extending the formalism presented in Ref. 36. We can summarize the result in the following way: Within the point contact model, defining $v^{r(1)} = \hbar \Gamma^{r(1)}$, one finds^{31;33}

$$P_{\beta=1}(v^r; v^1) = \frac{1}{2(1-f^2)^{1/2}(v^r v^1)^{1/2}} \exp \left[-\frac{v^r + v^1}{2(1-f^2)} \right] \cosh \left[\frac{2f \sqrt{v^r v^1}}{1-f^2} \right]; \quad (18)$$

where $f = AC(k, r; E) = J_0(kr)$ in two dimensions. For $f = 0$ one immediately realizes that the standard product of Porter-Thom as distributions is recovered. Unfortunately, we did not succeed in computing analytically the conductance peak height distribution starting from Eq. (18). However, it is rather straightforward to express the average conductance as a function of f in terms of special functions. To leading order in powers of f^2 one finds

$$\langle h(k, r) \rangle_{i=1} = \frac{1}{4} \left(1 + \frac{3}{4} [J_0(kr)]^2 \right) + O(f^4); \quad (19)$$

For $kr \ll 1$ we recover the average predicted by Eq. (8), as we should. In a typical experiment, by adding electrons and changing k, r , $\langle h(k, r) \rangle$ becomes a slowly oscillatory function on the energy scale of peak spacings. These long range oscillations in $\langle h \rangle$ do not appreciably change the autocorrelation function $c(n)$ for small n , being only pronounced at the tails. These statement is in agreement with the results shown in Ref. 35. By identifying $k = k_F$ (the Fermi wave number) and taking a typical experimental value for $k_F r$, the amplitude of the modulation will be of the order 1% of the standard RMT value for $\langle h \rangle$. This means that the maximum anticorrelation in $c(n)$, at $n = n_{\text{anti}}$, is also about 1% of $c(0)$.

A similar calculation can be made for the case of unitary symmetry ($\beta = 2$). Also in this case the joint probability distribution has already been derived^{32,33} and reads

$$P_{\beta=2}(v^r; v^l) = \frac{1}{1 - f^2} \exp \left(-\frac{v^l + v^r}{1 - f^2} \right) I_0 \left(\frac{2f \sqrt{v^r v^l}}{1 - f^2} \right); \quad (20)$$

where $I_0(x)$ is the modified Bessel function. Here, again, it is difficult to obtain the conductance peak height distribution $P(h)$ in a closed form. The averaged $\langle h \rangle$ as a function of f , on the other hand, can be found without much effort. The result in ascending powers of f^2 reads

$$\langle h(k, r) \rangle_{i=2} = \frac{1}{3} \left(1 + \frac{2}{5} [J_0(kr)]^2 \right) + O(f^4); \quad (21)$$

which is an even smaller correction than for the orthogonal case.

In distinction to the findings of Ref. 35, such spatial correlation effects will be hardly observable at zero temperature. We attribute the difference between our results and theirs mainly to their stringent constraint of having an exact symmetry in the wave functions near the tunneling region. Nonetheless, we anticipate that the long-range autocorrelation oscillations become more pronounced with increasing temperature, as we show in our numerical calculations. For future comparison with experiments, it is important to notice that the presence of an obstacle between r_1 and r_2 just requires the replacement of r by the length of the shortest classical path connecting r_1 to r_2 .³⁷ Before concluding, an additional comment is in order. Until the present, Coulomb blockade experiments have offered very few fingerprints of the underlying classical electronic dynamics. An experimental check of the effect proposed in Ref. 35, exploring the symmetries of the wave function, would offer a clear indication of the validity range of the single-particle approximation and the semiclassical analysis.

B. Non-universal dynamical correlations due to scars

Strong wave function correlations due to classical structures in phase (and coordinate) space, such as scars,³⁴ can also lead to a non-universal behavior in the peak height fluctuations.³⁸ The analysis presented in this section is motivated by a recent work of Hackenbroich and collaborators²⁷ which explored the idea of shape deformation to explain correlations between heights of neighboring peaks. These authors proposed a correlation mechanism tailored for integrable systems. In what follows, we recast and reinterpret their mechanism for chaotic systems with strong scarring. Our results for this case are qualitatively distinct from those of Ref. 27.

For an integrable system it is well known that the structure of a given wave function does not change upon a parametric variation of the Hamiltonian. The reason is quite simple. The wave functions of integrable systems are strongly concentrated around classical tori, and the latter are only smoothly distorted by a parametric variation of the Hamiltonian. This behavior is generic, provided the system stays integrable upon the parametric variation. However, as the parameter X is varied, levels cross each other. Since they correspond to different sets of quantum numbers, the typical crossing distance is much smaller than the distance necessary to appreciably change the wave functions. Let us assume that in certain system there are levels very weakly influenced by changes in X . We call them "horizontal" levels h . (Any h level certainly has a quite marked wave function structure with respect to the system geometry.) "Horizontal" levels may cross generic levels, as the parameter X is varied. Let us assume now that the conductance peak of a dot containing N electrons is dominated by a certain h level for some value of X . If the typical ΔX caused by the addition of one extra electron to the dot is of the order of the average parametric distance between crossings, the h level will always stay very close to the Fermi energy. In this way, the sequence of conductance peaks are dominated by the very same "horizontal" level and are thus expected to show correlations in heights. This mechanism²⁷ is robust as long as the system dynamics is close to integrable. The restrictive condition of having exactly one anticrossing for ΔX can be relaxed if temperature is included.²⁵

In the case of chaotic systems, wave functions typically decorrelate after one level crossing.³⁹ Deviations of such universal behavior indicate the presence of scarred eigenstates. For such wave functions the mechanism described in the previous paragraph is applicable. However, one should be aware that if peak height correlations are explained by a non-universal feature they are not ubiquitous.

In what follows we shall exemplify such mechanism and investigate how often these situation occurs. Moreover, by changing shape, position of the contacts, and temperature, we nearly exhaust all sources of peak height correlations within the single-particle scenario. The results are compared with those of RMT and the available experimental data.

C. Dynamical model: the smooth stadium potential

In order to investigate both aforementioned mechanisms, we studied the two-dimensional model Hamiltonian $H = p^2/2 + V(r)$ (we take the electron mass $m = 1$), with the potential given by⁴⁰

$$V(x,y) = \begin{cases} \frac{1}{2} \left(\frac{x^2}{a^2} + \frac{y^{2n}}{a^2} \right) & |x| \leq a, |y| \leq 1 \\ 1 & |x| > a \text{ or } |y| > 1 \end{cases} \quad (22)$$

The exponent n sets the steepness of the confining potential. The model is flexible enough to allow for different classical behaviors. For instance, if we take $n = 1$ the system is integrable. As we increase the value of n our model Hamiltonian becomes very similar to the well-known stadium billiard, one of the paradigms of classical chaotic systems. For $a = 1$ the equipotential $V(x,y) = 1$ corresponds to the border of the hard-walled stadium billiard with unit radius and unit rectangular length.

The model changes in the single-particle potential by varying a , the length of the rectangular part of the well. The classical motion is chaotic if a is varied in the interval range $1.0 < a < 1.25$, provided we choose $n = 2$ and stay in the energy window around $E = 1$. Indeed, for this energy and parameter values the classical phase space is mostly chaotic, as can be seen in Fig. 7, though small remnants of integrability still exist.

Finally, to assure that the single-particle levels we analyze correspond to a classically chaotic motion, we wish in order to have a window of energy around $E = 1$ containing typically 100 eigenstates of our Hamiltonian. The quantum eigenstates are obtained by numerical diagonalization. The problem is solved by using as basis states the eigenfunctions of a sufficiently large rectangular box. When the index n is an integer number, the calculation of the matrix elements is straightforward. The secular matrices are taken large enough such as to guarantee the convergence of all eigenvalues we analyze within 1% of the mean level spacing. This gives us confidence that the computed wave functions have converged. After ordering the eigenvalues in ascending energies, we consider only the eigenstates between the 200th and the 300th levels. A representative region of the spectrum of the smooth stadium with $n = 2$, in the absence of an external magnetic field, is shown in Fig. 8.

Quantum calculations including a magnetic field B perpendicular to the stadium are also of simple implementation in this model. By the usual minimum ansatz $\mathbf{p} \rightarrow \mathbf{p} + e\mathbf{A}(\mathbf{r})/c$ with $B = \nabla \cdot \mathbf{A}$ we obtain a new Hamiltonian that can be diagonalized following the same numerical procedure. We found useful to work in the gauge where $A_x = B/2[y - y_0]$; $A_y = B/2[x - x_0]$ with $c_x + c_y = 2.0$. Of course, the converged results do not depend on a particular choice of the gauge. However, the numerics can be made more efficient by choosing (x_0, y_0) close to the geometrical center of the stadium and $c_x L_x = c_y L_y$, where L_x and L_y are the lengths of the classically allowed region of the billiard at $E = 1$. With this choice, we obtain the largest ratio of number of converged eigenvalues to size of the secular matrix. We followed Ref. 41 to estimate the magnitude of the time-reversal breaking magnetic flux Φ_c threading the stadium. At the Fermi energy we obtain $\Phi_c = \Phi_0/2$, where Φ_0 is the unit flux quantum. When comparing the results of the dynamical model against the RMT unitary case, we fix the magnetic field to be $B A = \Phi_c$, where A is the classical allowed area for an electron with energy E_F .

Although the system is chaotic, there are many very narrow avoided crossings, which are characterized by a gap. These crossings occur for only a few eigenstates, indicating that the latter are very weakly coupled to others eigenstates. This non-universal feature is well-known in quantum chaos and is a fingerprint of scarred wave functions. Scarred eigenstates have the property of concentrating wave function amplitudes along certain classical

periodic orbits. Upon a parametric variation and after a level crossing, scarred eigenstates preserve their strong identity. In view of Fig. 8, we can apply the mechanism proposed for integrable systems in Ref. 27 to explain strong peak-to-peak correlations. We identify the n levels with scarred "horizontal" states. The states that contribute to the conductance in the case where $X = X_c$ and $k_B T$ are indicated in Fig. 8 by dots. The two sequences shown correspond to different Fermi energies. The wave functions related to the lower energy sequence are concentrated along the family of periodic orbits that bounce from $y = 0$ to $y = 1$ with $v_x = 0$ (the so called bouncing ball modes). The corresponding conductance peak heights show very large peak-to-peak correlations when the leads are placed such as to intersect these bouncing trajectories. The result is shown in Fig. 9. Notice that for small temperatures the mechanism holds even if the scarred state does not correspond to the Fermi level, but is its neighbor. This happens because scarred levels show very weak level repulsion and very often contribute significantly to the canonical occupation factor at $k_B T$. Differences in $c(n)$ due to spectral fluctuations were already discussed in III).

The proposed mechanism holds for chaotic systems if three main conditions are met. First, the tunneling state at the Fermi energy has to be localized in coordinate space. Second, X has to be close to X_c to keep this state close to ψ_F . Third, the leads have to be in the region where the wave function has an enhanced amplitude. In practice, these conditions are obviously difficult to be satisfied simultaneously. However, one could imagine that a given sequence can have few correlated peaks dominated by a particular scarred state. When this state drifts away from the Fermi level it will eventually be replaced by another localized state. In this way a peak height sequence would have several regions where peaks are strongly correlated. This is the kind of effect that we actually tried to identify. Although we observed sequences like that in the numerical simulations, the proposed mechanism is not generically robust. When one averages over many sequences by varying the positions of the contacts inside the billiard, the Fermi level, as well as X_c . The autocorrelation functions $c(n)$ dependence on $k_B T$ does not differ much from the RMT result. In other words, sequences like the top one in Fig. 8 are statistically dominant.

Summarizing: chaotic systems like the stadium can, in some cases, display strong peak-to-peak correlations. Such cases, however, are statistically rare and in our opinion this mechanism is not robust enough to explain the experimental data.^{9,13}

Let us now turn to the study of long range correlations. For this purpose we evaluated $c(n)$ for the smooth stadium without magnetic field. Deformations which cause energy levels to change by ϵ are very small at the classical level and do not influence our results. We therefore only consider the case of $X = 0$. The data set consists of 60 sequences of 100 peaks each. The peaks in each sequence are normalized to unit average height. This is done to avoid the systematic errors due to the decrease of the mean conductance from one sequence to another (since each sequence corresponds to a different length a). A correlator is calculated for each sequence and an average over all sequences is taken. For $k_B T = 0$ no undershooting is observed in $c(n)$, as predicted in Sec. IV A. The results for $k_B T = 0.5$ are shown in Fig. 10. We do not know how to estimate the magnitude of the oscillations in $c(n)$ after the temperature average, since f enters in the expressions in a convoluted manner. In Fig. 10 we observe much larger oscillations than predicted by the theory at $k_B T = 0$. We can check if the enhanced oscillations are related to the mechanism proposed in IV A, by verifying if n_{anti} (the position of the anticorrelation maximum) is consistent with our theory.

Our data were obtained by sweeping k_F and keeping the lead positions fixed. For spinless electrons in a billiard, $k_F \propto (4N/A)^{1/2}$. To add one electron to the dot, we have to move up in energy by ϵ in our model. This corresponds to change k_F by $2\epsilon/Ak_F$. Using the parameters of our calculations, we then estimate the position of the maximal anticorrelation to be $n_{\text{anti}} \approx 8$, which has to be contrasted with Fig. 10. A similar exercise was done in Ref. 35 using realistic values to estimate n_{anti} from the experimental data, obtaining values in reasonable agreement with Ref. 13. In our work, anticorrelations in $c(n)$ cannot be ruled out for small values of $k_B T$; nevertheless, they have to increase at higher temperatures and this is observed in our numerical simulations. We postpone the presentation of this result to the next section, where we also discuss the possible statistical problems inherent to such study.

V. FINITE DATA SET AND THE PEAK HEIGHT AUTOCORRELATION FUNCTION

The proper statistical treatment of experimental data is of great importance in any fluctuation analysis. In practical situations the number of Coulomb blockade peaks in a sequence goes from 50 to 100. Therefore, the problem of biases and errors due to finite sample size is one of the major difficulties in calculating peak height autocorrelation functions. If a reliable estimate of the effective number of independent points N_e can be made, the problem of making corrections and estimating errors is partially solved.

Considerable effort was devoted to this type of problem in the context of compound nucleus reactions (see, for instance, Ref. 42 and references therein). In this case the observable of interest is the nuclear cross section, whose autocorrelation function is known to be Lorentzian. Let us translate this earlier estimate for the effective number of independent peaks into the language of Coulomb blockade. For this purpose, we assume momentarily that the peak height autocorrelation function has a Lorentzian shape. Doing so and introducing $r = n/n_c$, we can write the variance of the average conductance peak height as

$$\text{var}(\bar{\Gamma}) = \text{var}(\Gamma) \frac{2 \tan^{-1} r}{r} \frac{\ln(1 + r^2)}{r^2} \quad ; \quad (23)$$

where $\text{var}(\Gamma)$ is the variance of the conductance peak height (either the "true" variance or, for an estimate, the ensemble variance), whereas $\bar{\Gamma}$ is the average over a sequence of n peaks with a correlation length n_c . It is known that if an average of N_e independent data points is computed, the variance of this average is given by

$$\text{var}(\bar{\Gamma}) = \frac{\text{var}(\Gamma)}{N_e} \quad ; \quad (24)$$

By comparing the two last equations, we can express N_e in terms of n/n_c . For values of $n/n_c \gg 1$, N_e is very well approximated by

$$N_e \approx \frac{1}{n/n_c} \quad ; \quad (25)$$

which tells us that an effectively independent point is found after an interval of n_c peaks. The statistical fluctuations are, as usual, given by $1/\sqrt{N_e}$. We expect our estimate of the number of effectively independent points to change little when a different functional form for the autocorrelation function is considered. The factor $\sqrt{2}$ will be replaced by another numerical factor of the same order of magnitude.

We illustrate this discussion by considering peak height autocorrelation functions obtained from sequences of different lengths for the smooth stadium without magnetic field or deformation for $k_B T = 0.5$ and 2 . As temperature increases, so does n_c ; statistical fluctuations become large even for samples with many peaks. This is illustrated in Fig. 11. At $k_B T = 2$, $n_c = 5$ and each sequence of 25 peaks has $N_e = 1$ and fluctuations prevail at $n = 1$. Similar results are obtained when a magnetic field is included, but are not shown here.

Notice that the correlation length is more sensitive to small samples at high temperatures. For instance, at $k_B T = 2$, n_c decreases appreciably as we consider shorter sequences. However, at $k_B T = 0.5$ the correlation length (defined as the HWHM) is stable. As a consequence, the curve $n_c(T)$ obtained from short sequences tends to saturate at high temperatures. This is similar to what is seen in Ref. 13 for the dot with $\epsilon = 38$ eV (Dot 2), the smallest one among the three dots tested. Our conclusion is that it is rather difficult to determine unambiguously that the saturation of n_c with temperature is a manifestation of decoherence. It may well be the effect of small statistics.

VI. ARE CONDUCTANCE FLUCTUATIONS A FINGERPRINT OF CLASSICAL CHAOS?

Any systematic search in the literature for single-particle models designed to explain the fluctuations of Coulomb blockade peak heights will reveal a strong bias towards the assumption of chaos. Very little attention has been devoted to integrable models, with, to the best of our knowledge, one exception.⁴³ This is quite understandable since it is believed that, due to small irregularities in the confining potential or the presence of weak impurities, the electronic dynamics tends to be chaotic. In fact, it is particularly difficult to set up an experimental realization of an integrable system. This statement is corroborated by the fact that there is only one kind of conductance experiment that shows a clear distinction between integrable and chaotic underlying dynamics.⁴⁴ However, this study, carried out by Chang and collaborators, dealt with the weak localization peak in open quantum dots, i.e., not in the Coulomb blockade regime.

Looking for clear fingerprints of integrable dynamics in the statistics of conductance in the Coulomb blockade regime is probably not a well posed task. Integrable systems are not universal, implying that each different confining potential will likely lead to very different conductance fluctuations. In this section we pursue the opposite strategy, asking if it is possible to tell from the conductance experimental data if the underlying dynamics is chaotic or not. To obtain some insight into this question we analyze two very simple systems, namely, the rectangular billiard (a paradigm of integrable motion) and the smooth stadium with $n = 1$.

We model the coupling of the quantum dot to a given lead by a point contact at the

position r_c , which implies that the decay width of the p th state is proportional to $j_p(r_c)^2$. For billiards it is standard to solve the single-particle problem with Neumann boundary conditions and to put the point contacts at the boundary.^{43;36} For chaotic system one obtains equivalent results choosing the point contacts inside the dot, thus probing the "bulk" of the single-particle wave functions. In this section we investigate both schemes.

For the rectangular billiard we can only proceed analytically in the regime where $k_B T \ll \epsilon_F$. The decay width of a state with quantum numbers $(n; m)$ is given by $\Gamma = (4/L_x L_y) \sin^2(k_n x) \sin^2(k_m y)$, up to a penetration factor. In the absence of an external magnetic field, in the "bulk" point contact model, $P(\epsilon)$ can be calculated through the expression

$$P_{\text{bulk}}(\epsilon) = \frac{1}{L_x L_y} \int_0^{L_x} dx \int_0^{L_y} dy \frac{4}{L_x L_y} \sin^2(k_n x) \sin^2(k_m y) : \quad (26)$$

For point contacts, one immediately obtains $\overline{h} = (L_x L_y)^{-1}$. The integrals in Eq. (26) represent an average over the position of the point contact. One could object that this is not the kind of average taken in experiments. However, it turns out that by reducing the integration in Eq. (26) to a single period in x and y , the wave function quantum numbers drop out of the integral and $P(\epsilon)$ becomes independent of n and m . In this sense, we claim that the average in Eq. (26) is equivalent to an average over a large number of wave functions with a fixed point contact position.

Performing the integral in Eq. (26) and writing the result in terms of \overline{h} , we arrive at

$$P_{\text{bulk}}(\epsilon) = \frac{1}{2} \frac{1}{\overline{h}} \int_0^1 dz \frac{1}{(1-z^2)(z^2 - 4\overline{h}\epsilon)}; \quad (27)$$

which can be written in a closed form in terms of a complete elliptic integral of the first kind (not shown here).

In a similar manner, we can calculate the distribution of decay widths $P(\epsilon)$ for the rectangular billiard with point contacts placed at its sides, obtaining

$$P_{\text{side}}(\epsilon) = \frac{1}{2} \frac{1}{\overline{h}} \int_0^1 dz \frac{1}{(2\overline{h}\epsilon - z^2)} : \quad (28)$$

In Fig. 12 we compare the analytical results of $P(\epsilon)$ for the rectangle with the Porter-Thomson distribution, which is the RMT prediction for the orthogonal symmetry. In addition, we also display the numerical results for the smooth integrable stadium potential ($n = 1$).

The similarity between the bulk rectangle and the smooth stadium with the Porter-Thomson distribution (in the absence of magnetic field) can be understood by a simple argument. Any wave function has a discrete number of points where its amplitude squared is a local maximum. It has also nodal lines where the amplitude is zero. By picking coordinates at random, the probability for obtaining a small amplitude is much bigger than for a large amplitude. It has to be emphasized, however, that neither the bulk rectangle nor the smooth stadium are in perfect agreement with the Porter-Thomson distribution. Although similar,

there are differences that can be better visualized in a log-log plot (not presented here), as shown before in the quantum chaos literature (see, for example, Ref. 43).

The most interesting aspect of this analysis appears when we treat the distribution of conductance peak heights $P(h)$. We find that $P(h)$ is relatively insensitive to $P(\epsilon)$, as illustrated in Fig. 13. Analytical calculations are rather difficult in this case, since, in general, we do not know how to take into account correlations between the decay widths Γ^1 and Γ^2 for integrable systems. Thus, the presented results were obtained numerically. Notice that although the histograms are somewhat different from the RMT result, they become indistinguishable when the usual experimental uncertainties (5-10%) are involved. (To construct the histogram shown in Fig. 13 we have used a very large sample of conductance peak heights.) The apparent similarity between the RMT prediction and the result for integrable systems becomes even stronger if we take $k_B T = 0.5$, as illustrated in Fig. 13b.

From this analysis, we conclude that the universal aspect observed experimentally for $P(h)$ is more robust than initially predicted. We believe that there is a large class of integrable systems which lead to conductance peak distributions similar to RMT. This result is not very intuitive, since for most observables integrable systems show larger fluctuations than chaotic ones.⁴⁵ We caution that our statement is not that any integrable system will display $P(h)$ similar to Eqs. (8) and (9). The literature already offers us a counter example: The conductance fluctuations observed in the model analyzed in Ref. 25 are certainly not compatible with RMT.

VII. CONCLUSIONS

In this work we aimed to study quantitatively how Coulomb blockade conductance peak statistics can be understood within the single-particle plus constant interaction model. We showed that the distribution of peak heights predicted by the RMT is very robust to deformations in the dot effective potential. For $k_B T > 0.25$ we found that there are exist integrable systems which give equivalent results to RMT. The curves derived numerically from RMT reproduce fairly the experimental results at low temperatures (for $k_B T < 0.5$), with increasing discrepancies as temperatures rises.

We also showed that the peak height long-range correlations can be understood in terms universal wave function correlations. The short range correlations remain an open problem. Under certain circumstances, we were able to reproduce peak sequences with visible bunching of peak heights. Their correlation lengths depend on the specific portion of the spectrum considered and is thus nonuniversal. Unfortunately, such sequences are relatively rare, since they rely on the existence of well-connected scarred states.

Starting from non-degenerate sequences of eigenenergies and tunneling rates, one can construct spin-degenerate data sets by simply duplicating the original sequences. In this case, at $k_B T = 0$ the conductance peaks should appear in pairs of equal heights. More importantly, paired peaks would have a similar response to external perturbations, such as a magnetic field, even if their heights are not quite identical. Experimentally, however, this behavior is not observed (with the possible exception of Fig. 2 in Ref. 13). In view of this fact, we have decided for restricting our analysis to nondegenerate single-particle levels.

It is noteworthy that the experiment by Chang and collaborators⁸ is the only one where

peak bunching is not visually strong. The main difference between the setup of Ref. 8 and others is the sample, which in this case has lower mobility. Disorder destroys the dynamical effects we propose. One could then speculate that the lack of peak height correlations in Ref. 8, and, perhaps, the departure from universality seen in other experiments depend on the strength of dynamical effects. From this perspective, our main conclusion is negative, since, we were not able to identify a robust mechanism to explain such phenomena based on this idea.

The hypothesis that the ground state and the excited states are uncorrelated and follow RMT leads always to the suppression of small conductance peak heights upon thermal averaging. Even the inclusion of additional features, like deformations, does not change this conclusion. In view of the experimental evidences of an even larger suppression of the small peaks than predicted by RMT, we might conclude that the ground state and the first excited states have instead some correlation. The mechanism responsible for this could also be responsible for the correlations between ground states with consecutive number of electrons. Thus, peak bunching and the persistence of small peaks could be manifestations of the same mechanism. From our analysis, however, such mechanism seems to be beyond the mean-field scenario. In conclusion, we believe that the full quantitative understanding of these effects may lay outside the single-particle approximation.

ACKNOWLEDGMENTS

We thank C. Marcus and S. Patel for making the experimental data on the conductance peak sequences available to us. Discussions with R. Jalabert, J. Richter, S. Tomsovic, and H. A. Weidenmüller were greatly appreciated. One of us (C.H.L.) thanks the hospitality of the Theoretical Physics Laboratory at the University of Strasbourg, where this work was concluded. We gratefully acknowledge the financial support of FAPERJ, CNPq, and PRONEX (Brazil).

REFERENCES

- ¹ M .K astner, Rev.M od.Phys. 64, 849 (1992).
- ² L.P.K ouwenhoven, C.M .M arcus, P.L.M cEuen, S.Tanucha, R.M .W estervelt, and N.S.W ingreen, in Mesoscopic Electron Transport, NATO ASI Series E, vol. 345, edited by L.P.K ouwenhoven, G .Schon, and L.L.Sohn (K luer, D ordrecht, 1997).
- ³ C.W .J.Beenakker, Rev.M od.Phys. 69, 731 (1997).
- ⁴ T.G uhr, H.A .W eidenm üller, and A.M üller-G roeling, Phys.Rep. 299, 189 (1998).
- ⁵ C.W .J.Beenakker, Phys.Rev.B 44, 1646 (1991).
- ⁶ R.A .Jalabert, A.D .Stone, and Y.A Ihassid, Phys.Rev.Lett. 68, 3468 (1992).
- ⁷ V.N.P rigodin, K.B.E fetov, and S.Ida, Phys.Rev.Lett. 71, 1230 (1993).
- ⁸ A.M .Chang, H.U .Baranger, L.N.P fei er, K.W .W est, and T.Y .Chang, Phys.Rev.Lett. 76, 1695 (1996).
- ⁹ J.A .Folk, S.R.Patel, S.F.G odijn, A.G .Huibers, S.M .Cronenwett, C.M .M arcus, K.Campm an, and A.C.G ossard, Phys.Rev.Lett. 76, 1699 (1996).
- ¹⁰ U.Sivam , R.Berkovits, Y.A loni, O .P rus, A.Auerbach, and G .Ben-Yoseph, Phys.Rev.Lett. 77, 1123 (1996).
- ¹¹ F.Sim mel, T.Heinzel, and D.A .W haram , Europhys.Lett. 38, 123 (1997).
- ¹² S.R.Patel, S.M .Cronenwett, D.R.D unuoz, J.S.Harris Jr., K.Campm an, and A.C.G ossard, Phys.Rev.Lett. 80, 4522 (1998).
- ¹³ S.R.Patel, D.R.Stewart, C.M .M arcus, M .Gokoedag, Y.A Ihassid, A.D .Stone, C.I.D unuoz, and J.S.Harris Jr., Phys.Rev.Lett. 81, 5900 (1998).
- ¹⁴ R.O .Vallejs, C.H.Lewenkopf, and E.R.M ucciolo, Phys.Rev.Lett. 81, (1998).
- ¹⁵ L.I.G lazman and R.I.Shekhter, J.Phys.Conden.M atter 1, 5811 (1989).
- ¹⁶ R.Berkovits, Phys.Rev.Lett. 81, 2128 (1998).
- ¹⁷ S.Levit and D .O rgad, cond-m at/9901298 (1999).
- ¹⁸ L.Bonci and R.Berkovits, cond-m at/9901332 (1999).
- ¹⁹ P.N.W alker, G .M ontambaux, and Y.G efen, cond-m at/9902258 (1999).
- ²⁰ A.Cohen, K .Richter, and R.Berkovits, cond-m at/9902342 (1999).
- ²¹ Ya.M .B lanter, A.D .M irlin, and B.A .M uzykanstskii, Phys.Rev.Lett. 78, 2449 (1997).
- ²² R.Berkovits and B.L.A ltshuler, Phys.Rev.B 55, 5297 (1997).
- ²³ M .L.M ehta, Random M atrices (Academ ic Press, New York, 1991).
- ²⁴ Y.A Ihassid, M .Gokoedag, and A.D .Stone, Phys.Rev.B 58, 7524 (1998).
- ²⁵ R.Baltin, Y.G efen, G .Hackenbroich, and H.A .W eidenm üller, cond-m at/9807286 (1998).
- ²⁶ W .E.O m and, D .J.D ean, C.W .Johnson, G .H .Lang, and S.E.Koonin, Phys.Rev.C 49, 1422 (1994).
- ²⁷ G .Hackenbroich, W .D .Heiss, and H.A .W eidenm üller, Phys.Rev.Lett. 79, 127 (1997).
- ²⁸ F.Sim mel, D .Abusch-M agder, D.A .W haram , M .A .K astner, and J.P.K otthaus, cond-m at/9901274 (1999).
- ²⁹ B.D .Sim ons and B.L.A ltshuler, Phys.Rev.Lett. 70, 4063 (1993).
- ³⁰ M .V .Berry, J.Phys.A 10, 2083 (1977).
- ³¹ V.N.P rigodin, Phys.Rev.Lett. 74, 1566 (1995).
- ³² V.N.P rigodin, N.Tanigushi, A.Kudrolli, V.K idambi, and S.Sridhar, Phys.Rev.Lett. 75, 2392 (1995).
- ³³ M .Srednicki, Phys.Rev.E 54, 954 (1996).

- ³⁴ E. J. Heller, Phys. Rev. Lett. 53, 1515 (1984).
- ³⁵ E. Narimanov, N. R. Cernuti, H. U. Baranger, and S. Tomsovic, cond-mat/9812165 (1998).
- ³⁶ Y. Alhassid and C. H. Lewenkopf, Phys. Rev. B 55, 7749 (1997); Phys. Rev. Lett. 75, 3922 (1995).
- ³⁷ S. Hortikar and M. Srednicki, Phys. Rev. Lett. 80, 1646 (1998).
- ³⁸ M. Stopa, Physica B 251, 228 (1998).
- ³⁹ E. R. Mucciolo, A. V. Andreev, B. D. Simons, and V. N. Prigodin, Phys. Rev. Lett. 75, 1360 (1995)
- ⁴⁰ A. M. Ozorio de Almeida and J. S. Espinosa Ortiz (unpublished).
- ⁴¹ Z. Pluhar, H. A. Weidenmüller, J. A. Zuk, C. H. Lewenkopf, and F. J. Wegner, Ann. Phys. (N.Y.) 243, 1 (1995).
- ⁴² T. Ericson and T. Meyer-Kuckuk, Ann. Rev. Nucl. Sci. 16, 207 (1966).
- ⁴³ H. Bruus and A. D. Stone, Phys. Rev. B 50, 18275 (1994).
- ⁴⁴ A. M. Chang, H. U. Baranger, L. N. Pfeiffer, and K. W. West, Phys. Rev. Lett. 73, 2111 (1994).
- ⁴⁵ Y. Alhassid and M. Feingold, Phys. Rev. A 39, 374 (1989).

FIGURES

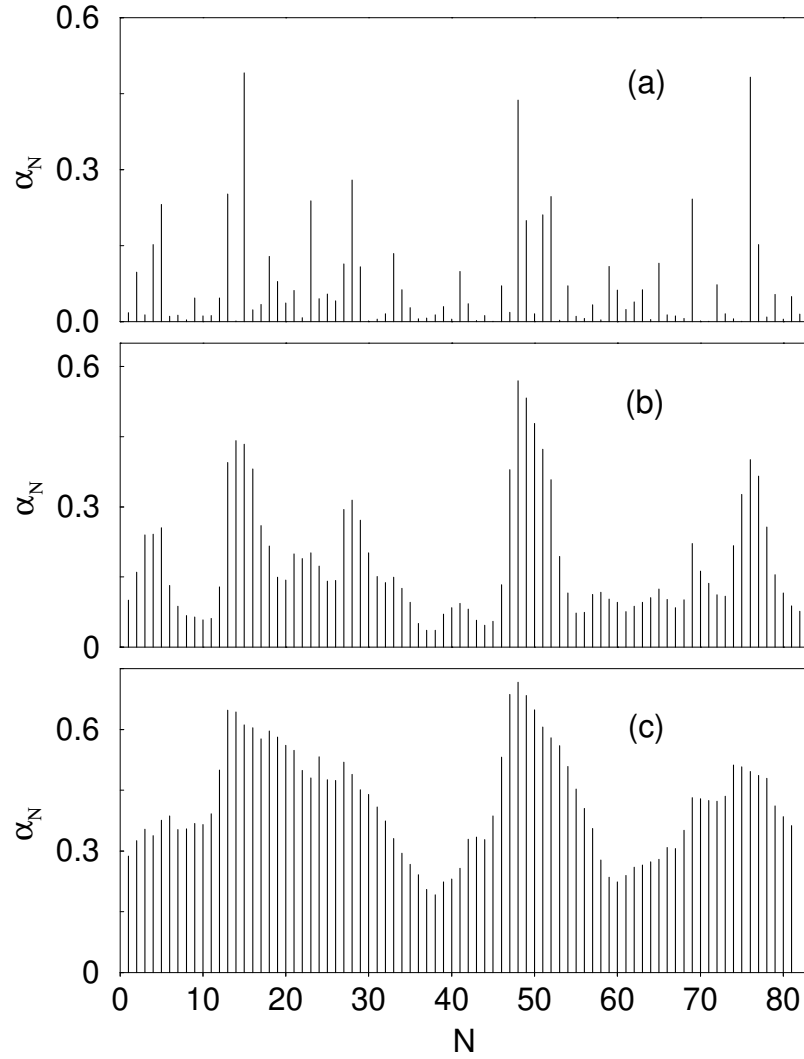


FIG .1. Sequences of dimensionless conductance peak maxima α_N taken from the GOE simulations for a given set of eigenstates and no deformation at (a) $k_B T = 0.1$, (b) $k_B T = 1$, and (c) $k_B T = 3$.

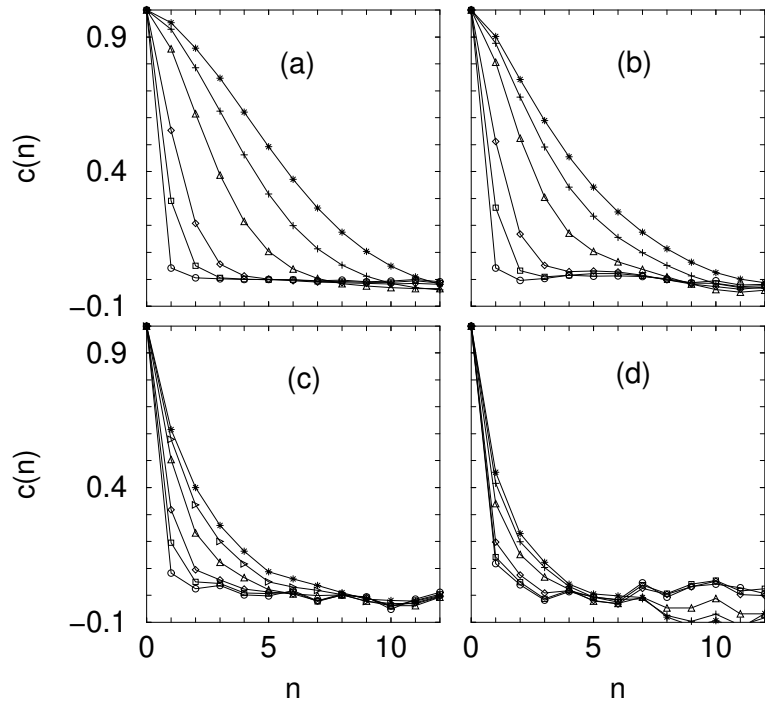


FIG. 2. Peak height correlation function for the GOE at temperatures $k_B T = 0.1$ (circles), 0.3 , 0.5 , 1.5 , 2 (stars) for different shape deformations: (a) $x = 0$, (b) $x = 0.1$, (c) $x = 0.5$, and (d) $x = 1.0$.

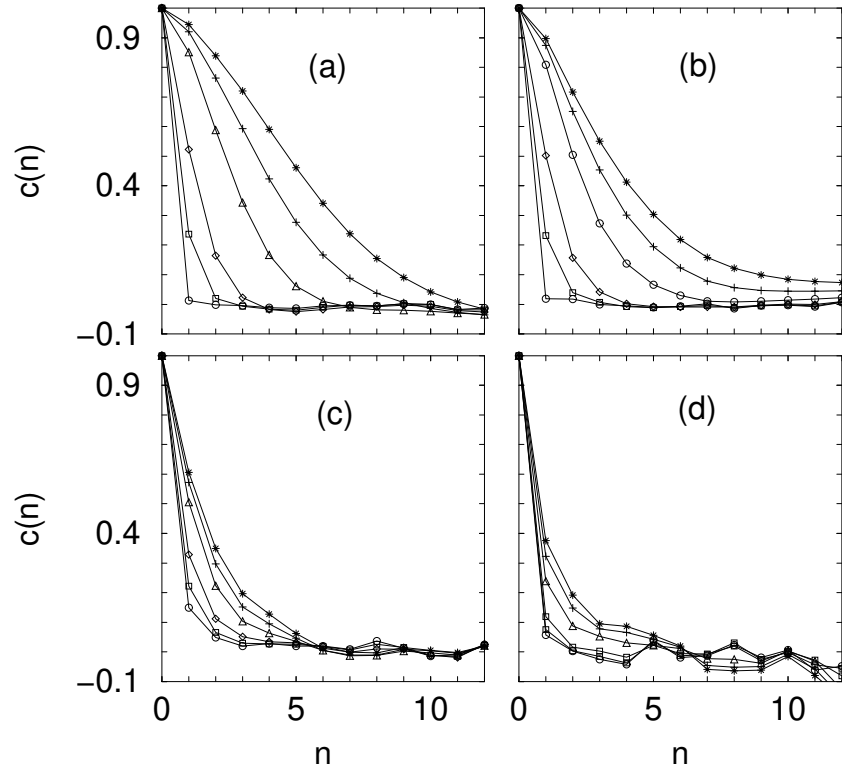


FIG .3. Same as in Fig.2, but for the GUE .

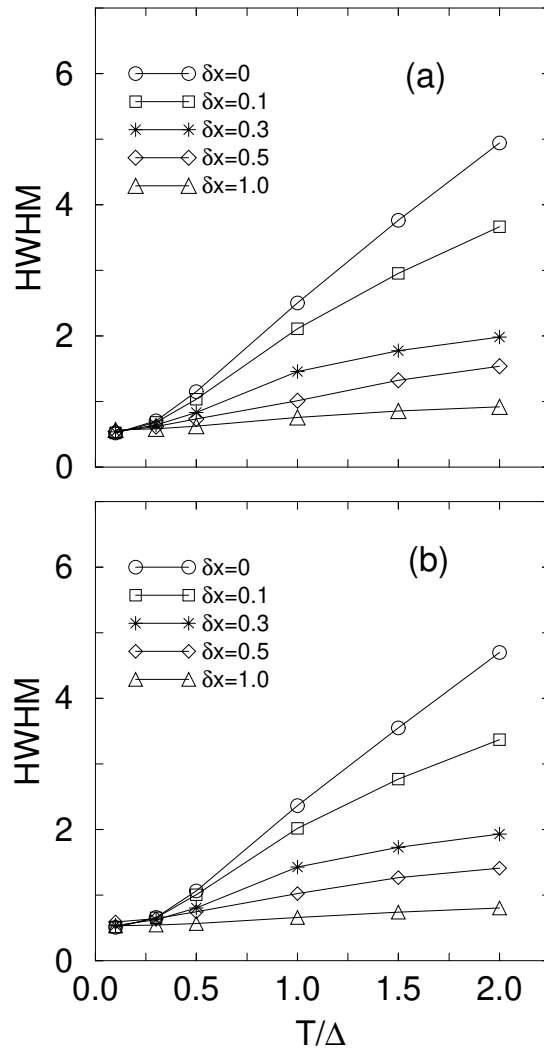


FIG .4. Correlation length (HWHM) obtained from Figs.2 and 3 for (a) GOE and (b) GUE.

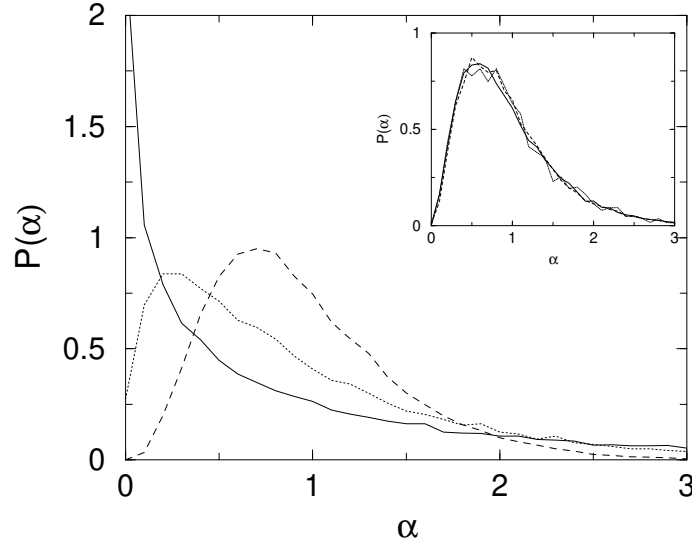


FIG. 5. Distribution of peak heights for the GOE without parametric distortion at different temperatures: $k_B T = 0.1$ (solid line), 0.5 (dotted line), and 1.5 (dashed line). The inset shows the distribution at $T = 0.5$ obtained for three different deformations ($x = 0.1, 0.3$, and 1.0). The heights are rescaled to $h_i = 1$.

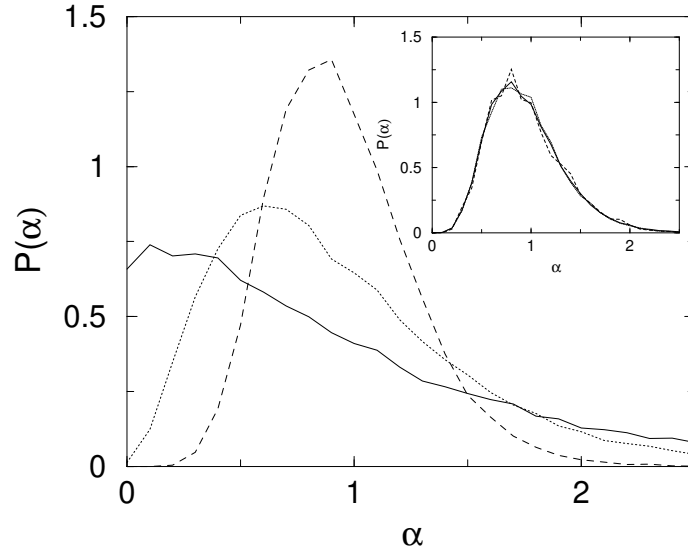


FIG .6. The same as in Fig.5 but for the GUE .

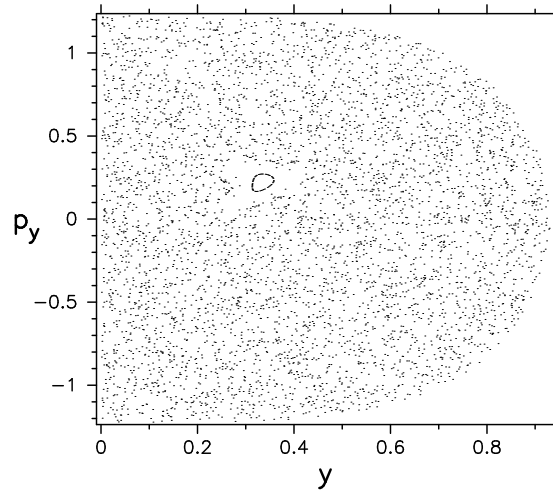


FIG .7. Poincare surface of section for the smooth stadium billiard with $n = 2$, $a = 1$, and $E = 0.75$. The section is taken at $x = a$.

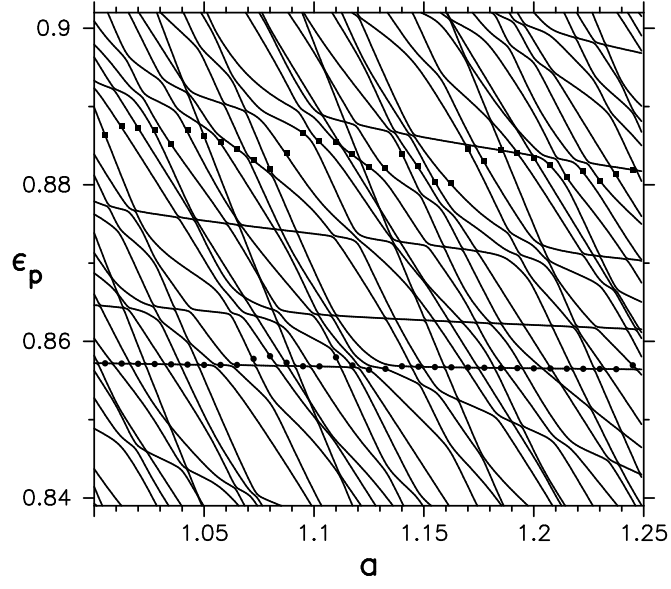


FIG .8. Energy levels as a function of the length a for the smooth stadium with $n = 2$ and no magnetic field. The two nearly horizontal sequences of dots correspond to tunneling states at low temperatures regime and for $x = 1$. The lower energy sequence follows a scarred pattern, while the higher one does not.

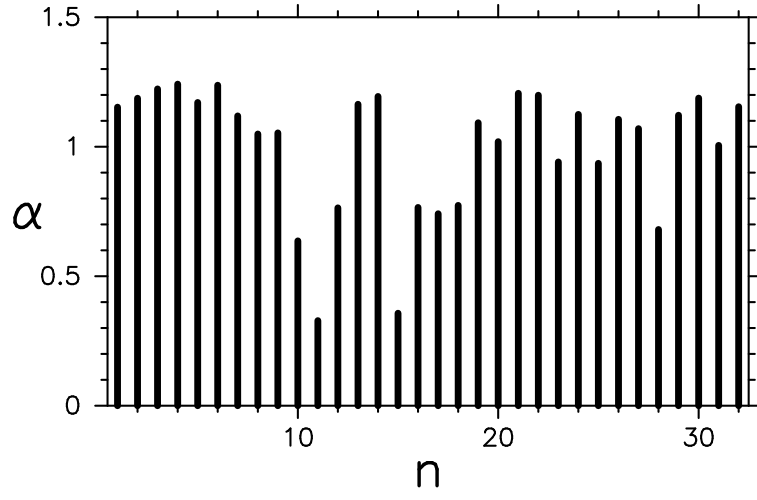


FIG . 9. Sequence of peak heights for "bouncing ball" wave functions at $k_B T = 0.25$.

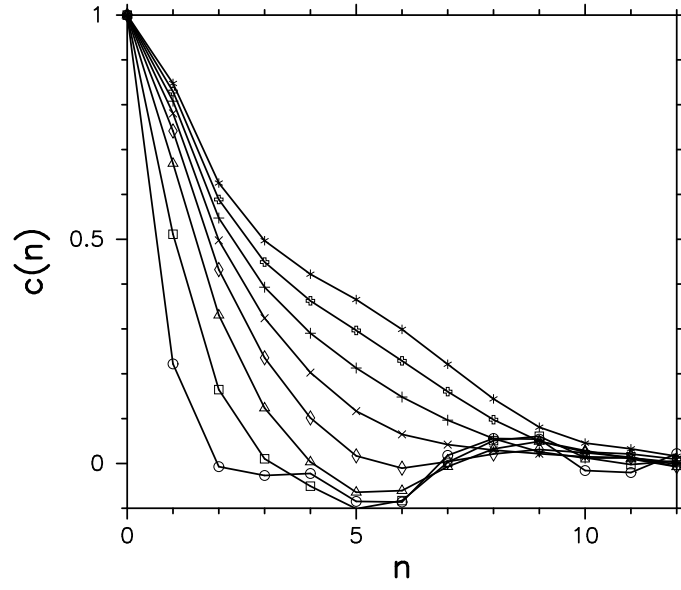


FIG .10. Peak height autocorrelation function $c(n)$ for the smooth stadium ($n = 2$, no magnetic field) obtained from 60 sequences of 100 peaks each, going from $k_B T = 0.25$ (circles) to 2 (stars) in increments of 0.25 .

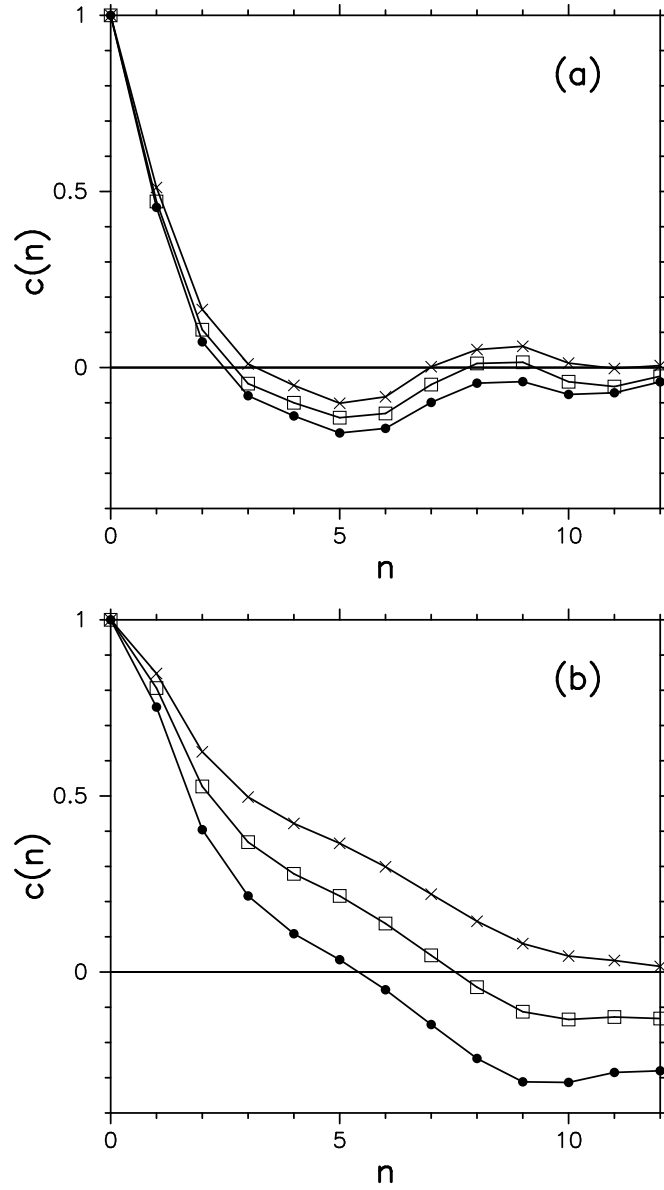


FIG. 11. Peak height autocorrelation function $c(n)$ for the smooth stadium obtained from different sets of sequences: 60 sequences of 100 peaks (crosses), 120 of 50 (squares), and 240 sequences of 25 peaks (circles). (a) $k_B T = 0.5$; (b) $k_B T = 2$.

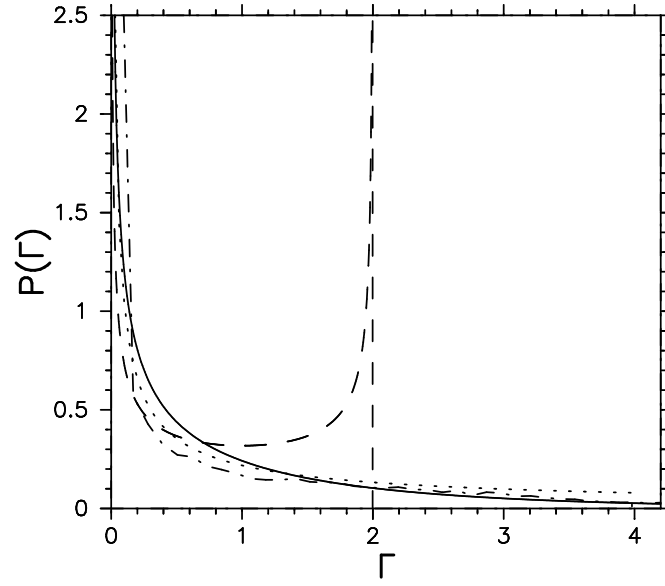


FIG. 12. $P(\Gamma)$ from RMT (solid line) compared with different integrable systems: bulk rectangle (dotted), side rectangle (dashed), and $n = 1$ smooth stadium (dash-dotted). The distributions are scaled to have $h_i = 1$.

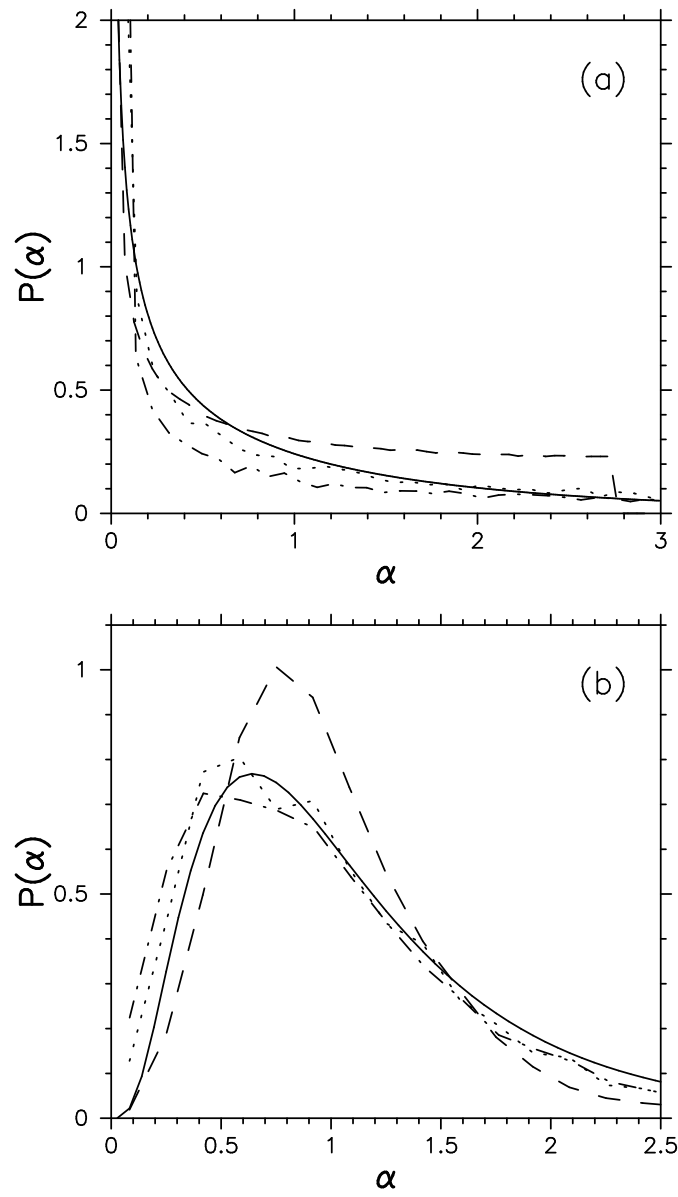


FIG. 13. $P(\alpha)$ from RMT (solid line) compared with different integrable systems: bulk rectangle (dotted), side rectangle (dashed), and $n=1$ smooth stadium (dash-dotted) for (a) $k_B T = 0$ and (b) $k_B T = 1.0$. The distributions are scaled to have $h_i = 1$.